AGU ADVANCING EARTH AND SPACE SCIENCE

Geophysical Research Letters

RESEARCH LETTER
10.1029/2020GL088997

Key Points:
- Intraseasonal salinity is better simulated by a high vertical resolution
- There is a regional dependency about physics controlling the MJO-related salinity variability
- The application of a coupled model other than ocean-only models is another uniqueness of this study

Supporting Information:
- Supporting Information S1

Correspondence to:
J. Zhu,
jieshun.zhu@noaa.gov

Citation:
Zhu, J., Kumar, A., & Wang, W. (2020). Intraseasonal surface salinity variability and the MJO in a climate model. *Geophysical Research Letters*, *47*, e2020GL088997. https://doi.org/10.1029/2020GL088997

Received 22 MAY 2020
Accepted 10 AUG 2020
Accepted article online 17 AUG 2020

Intraseasonal Surface Salinity Variability and the MJO in a Climate Model

Jieshun Zhu[1,2], Arun Kumar[1], and Wanqiu Wang[1]

[1]Climate Prediction Center, NOAA/NWS/NCEP, College Park, MD, USA, [2]Earth System Science Interdisciplinary Center, University of Maryland, College Park, MD, USA

Abstract Due to the sparsity of ocean observations, understanding inconsistencies exist even in qualitative respect about the mechanisms of intraseasonal sea surface salinity (SSS) over the Indo-Pacific basin. In this study, a quantitative diagnostic of salinity/freshwater budgets related to the Madden-Julian oscillation (MJO) was conducted based on model simulations. The model applied is a modified version of the NCEP Climate Forecast System, version 2. The application of a coupled model other than ocean-only models is one of the unique aspects of this study. The model modifications resulted in a more realistic MJO simulation and a better simulation of intraseasonal SSS variability as validated against the Aquarius estimates. The mechanisms of the MJO-related SSS variability are further explored by conducting a salinity budget analysis over the mixed layer. The analysis indicates a strong spatial variation of dominant physical processes controlling the local SSS variability. For example, while the role of surface fluxes dominates in the western Indian basin, oceanic advection plays an important role in the eastern Indian and western Pacific oceans.

1. Introduction

The Madden-Julian oscillation (MJO) (Madden & Julian, 1971) is the primary intraseasonal mode in the tropics during the boreal winter and spring. It is generally considered as an intrinsic mode of the tropical atmosphere (e.g., Wang & Rui, 1990), but the air-sea coupling is also suggested to be important for its dynamics (e.g., DeMott et al., 2015; Flatau et al., 1997). In observations, coherent variations have been seen in surface heat fluxes, sea surface temperature (SST), and convections associated with the MJO (e.g., DeMott et al., 2015; Krishnamurti et al., 1988; Kumar et al., 2013; Shinoda et al., 1998). In many numerical studies, the MJO is also better simulated when an ocean model is coupled to an atmosphere-only general circulation model (AGCM) (e.g., Flatau et al., 1997; Inness et al., 2003; Waliser et al., 1999; Zhang et al., 2006; Zhu et al., 2017), confirming the role of oceanic feedbacks in the MJO evolution. Furthermore, the inclusion of air-sea coupling was found to extend the MJO predictability and increase the capability of predicting the tropical intraseasonal oscillation (e.g., Fu et al., 2008; Pegion & Kirtman, 2008; Vitart et al. 2007; Zhu & Kumar, 2019). Thus, investigating the MJO-related oceanic variability is not only crucial for a better understanding of the MJO dynamics but also beneficial for its operational predictions.

In comparison with ocean salinity, most of the previous analyses focused on the MJO-related SST variability (particularly over the Indo-Pacific Ocean), and it is because of several reasons: SST can directly influence the overlying atmosphere while salinity cannot, resulting in more focus on MJO-SST interactions; historically, ocean temperature has been better observed than salinity. Regarding SST, numerical experiments suggest that the observed MJO-related SST anomalies could be largely reproduced by one-dimensional mixed layer models as a response to the observed MJO related surface heat flux anomalies (e.g., Shinoda & Hendon, 1998); however, wind stress-driven zonal advection also plays a role in the western Pacific (e.g., Shinoda & Hendon, 2001). Further studies (e.g., Zhang et al., 2010) indicated that the relative importance of the thermodynamic versus dynamical forcing has large spatial and temporal variations, which depends on the intensity of the MJO forcing and the ocean background state.

Ocean salinity, on the other hand, is another fundamental physical property of seawater that not only influences the stratification and circulation of the global oceans but is also a potential indicator of the global water cycle (e.g., Schmitt, 2008). In some ocean basins (e.g., the Indo-Pacific warm pool region) where the upper ocean stratification is largely controlled by salinity, the barrier layer (BL) exists between the base of

the density-defined mixed layer and the thermocline (Lukas & Lindstrom, 1991; Sprintall & Tomczak, 1992). The existence of BL could have significant climate influences (Cravatte et al., 2016). By modulating BL in the Indo-Pacific region, for example, salinity is suggested to influence the evolution of important climate modes, such as Indian Ocean Dipole (e.g., Annamalai et al., 2003), El Niño-Southern Oscillation (e.g., Maes et al., 2005; Zhu et al., 2014), and the Asian Monsoon (e.g., Seo et al., 2009). The feedback of salinity onto the MJO is also suggested via its modulation in upper ocean stratification variability (e.g., BL) and further in intraseasonal SSTs (e.g., Drushka et al., 2014; Guan et al., 2014).

Quantifying salinity variability is historically challenging due to the sparsity of its observations, but this issue is somewhat alleviated since the advent of Argo profiles (Roemmich & Owens, 2000) and satellite salinity missions (e.g., Aquarius, Lagerloef, 2012; SMOS, Font et al., 2013). On intraseasonal time scales, these new data sets have yielded new insights into salinity variability associated with the MJO (e.g., Drushka et al., 2012, 2014; Grunseich et al., 2013; Guan et al., 2014; Matthews et al., 2010; Shinoda et al., 2013). By a composite analysis of 4-year Argo float data, for instance, Matthews et al. (2010) found that the MJO-related sea surface salinity (SSS) anomalies are consistent with evaporation minus precipitation fluxes (E − P) in the Indian Ocean and with anomalous zonal advection in the Pacific. Based on Argo data as well, Drushka et al. (2014) evaluated the modulation of BL on the upper ocean response to the MJO forcing in the eastern equatorial Indian Ocean, and significant consequences were identified with thicker BLs corresponding to weaker SST anomalies. Grunseich et al. (2013) analyzed 18 months of Aquarius SSS data and concluded that MJO-related SSS anomalies in both the Indian Ocean and West Pacific were governed by E − P forcing. The Aquarius-based conclusion was updated by Guan et al. (2014), who found more complexity in salinity budget, with the MJO-related SSS variations attributed to the E − P forcing in the western Indian Ocean throughout the MJO life cycle and in the central Indian Ocean during the wet phase of the MJO cycle and implicitly attributed to ocean dynamics in the central Indian Ocean during the dry phase and in the eastern Indian and western Pacific Oceans throughout the MJO cycle. The observational diagnoses are also complemented by forced ocean simulation experiments (e.g., Li et al., 2015; Li & Han, 2016).

In general, the previous studies suggested significant modulations of upper-ocean salinity by the MJO, but inconsistencies in their results remain, even in qualitative respect, about the relative effect of E − P flux versus the of role ocean dynamics (Grunseich et al., 2013; Guan et al., 2014; Matthews et al., 2010). Most of the conclusions were drawn based on a qualitative description of patterns of SSS and E − P anomalies, with the role of ocean dynamics inferred implicitly.

To provide more insights about the MJO-related SSS anomalies, in this study, we provide a quantitative description of salinity/freshwater budgets related to the MJO, which has been hindered by sparse coverage of salinity observations together with a lack of high-quality three-dimensional ocean current observations. Our analysis is based on a coupled model simulation. The utility of coupled models in such an analysis is challenging because of long-standing model biases. For the MJO particularly, shortcomings remain in simulating its amplitude, period, seasonality, and geographical dependence (e.g., Hung et al., 2013; Jiang et al., 2015). A common shortcoming, for example, is that the eastward propagation of convections across the Maritime Continent is poorly represented in many general circulation models (GCMs) with standing oscillations of convective activity over the Indian Ocean or western Pacific (Jiang et al., 2015). Similar biases in the ocean are also evident in contemporary coupled GCMs (CGCMs). Zhu and Kumar (2019) identified large biases in simulating the climatological BL distribution and intraseasonal SSS variability in CFSv2 (Saha et al., 2014). These model deficiencies could limit the utility of CGCMs in scientific explorations. In this study, improved simulation of the MJO and intraseasonal SSS variability was achieved by applying modifications to the operational CFSv2 (Saha et al., 2014), and thus, the use of simulations based on this model results in a more realistic assessment of the SSS variability in different ocean basins.

2. Model, Experiments, and Analysis Methods

2.1. Model and experiments

The model used is the NCEP CFSv2 (Saha et al., 2014; see the supporting information for a brief description of CFSv2). In this paper, the operational version of CFSv2 (Saha et al., 2014) is referred to as CFSv2SAS to highlight its application of simplified Arakawa-Schubert scheme (SAS; Pan & Wu, 1995) for parameterizing atmospheric convections. For the application of CFSv2 in this study, two modifications were introduced in

the operational version. The first one is a replacement of its convection scheme with the relaxed Arakawa-Schubert (RAS; Moorthi & Suarez, 1992) scheme, and the configuration is referred to as CFSv2RAS to distinguish from CFSv2SAS. Zhu et al. (2017) suggested that the adoption of RAS significantly improves the MJO simulations, particularly its eastward propagation through the Maritime Continent.

The second model modification is an enhancement of ocean vertical resolution to 1 m near the ocean surface. In both CFSv2SAS and CFSv2RAS, the ocean component has a vertical resolution of 10 m for the upper 200 m, as in most climate models. Considering that a 10-m vertical resolution is too coarse to represent the mixed layer diurnal cycle (Bernie et al., 2005; Li et al., 2013) which has been suggested to be important in modulating MJO convection (e.g., Bellenger et al., 2010) and its prediction (e.g., Woolnough et al., 2007), the oceanic vertical resolution of CFSv2 was increased to 1 m near the ocean surface (the upper 10 m; Ge et al., 2017). To facilitate the resolution change, the oceanic component of CFSv2 is also replaced by the newer MOM5. The new configuration is hereafter referred to as CFSm501, which includes both atmospheric and oceanic modifications as described above. Zhang et al. (2019) found that the application of 1-m vertical resolution predicted intraseasonal SST anomalies with larger amplitudes and produced higher prediction skill in both intraseasonal SST and rainfall anomalies.

In this study, the above three CFSv2 configurations (i.e., CFSv2SAS, CFSv2RAS, and CFSm501) were integrated for more than 20 years, starting from a CFSR (Saha et al., 2010) initial state. All diagnostics are based on the last 15-year simulations by treating the early years as spin-up periods.

2.2. Mixed layer salinity budget analysis

To provide a quantitative description of the role of ocean dynamics versus E − P in intraseasonal salinity variability, a budget analysis is performed for mixed layer salinity in CFSm501. The budget analysis is formulated as follows (e.g., Cronin & McPhaden, 1998):

$$\frac{\partial S_a}{\partial t} = \frac{1}{h} S_0 (E - P) - \boldsymbol{v}_a \cdot \nabla S_a - \frac{1}{h} \nabla \cdot \int_{-h}^{0} \widehat{\boldsymbol{v}} \widehat{S} dz - \frac{1}{h} (S_a - S_{-h}) \left(\frac{dh}{dt} + w_{-h} \right) - \frac{1}{h} F_{-h}, \tag{1}$$

with symbols explained in the supporting information. As described in Cronin and McPhaden (1998), the local change in the vertically averaged salinity can be due to the dilution effect of the surface freshwater flux (evaporation minus precipitation), horizontal advection by the vertically averaged currents, stratified shear flow convergence, vertical entrainment process, and turbulent diffusions.

2.3. Data Sets

Some observations were adopted to validate model simulations, including daily SSS from the Aquarius Level 3 product based on the Combined Active-Passive algorithm (Yueh, 2013), rainfall estimate from the CPC CMORPH product (Joyce et al., 2004), and 850-hPa zonal winds from the CFSR (Saha et al., 2010). The MJO events in both observations and simulations are tracked by the real-time multivariate MJO (RMM) index (Wheeler & Hendon, 2004), with the observed daily RMM index values obtained through http://www.bom.gov.au/climate/mjo/. Validations are mostly made for January 1998 to December 2014 but for August 2011 to June 2015 (the Aquarius record period; Lagerloef, 2012) for SSS.

3. Results

As the focus of this study is the MJO-related SSS variability, a prerequisite for using model simulations is that the MJO is realistically simulated by the model. Figure 1 examines the simulated MJO features with three CFSv2 configurations, with the focus on its zonal propagation and is documented by the lag-longitude diagrams of equatorial properties regressed against the Indian Ocean precipitation.

In observations (Figure 1a), the MJO-related convection tends to propagate eastwards across the Maritime Continent from the eastern equatorial Indian Ocean to the western Pacific. Contemporaneous GCMs, however, still have different levels of fidelity in representing the propagation, and many of them simulate standing oscillations of convective activity over the Indian Ocean or western Pacific (e.g., Inness et al., 2003; Jiang et al., 2015). This propagation simulation bias is also present in CFSv2SAS (Wang et al., 2014; Zhu et al., 2017) in which the intraseasonal convection activity stops propagating when encountering the Maritime Continent (color shading in Figure 1b). Our previous studies (Zhu et al., 2017) suggested that the

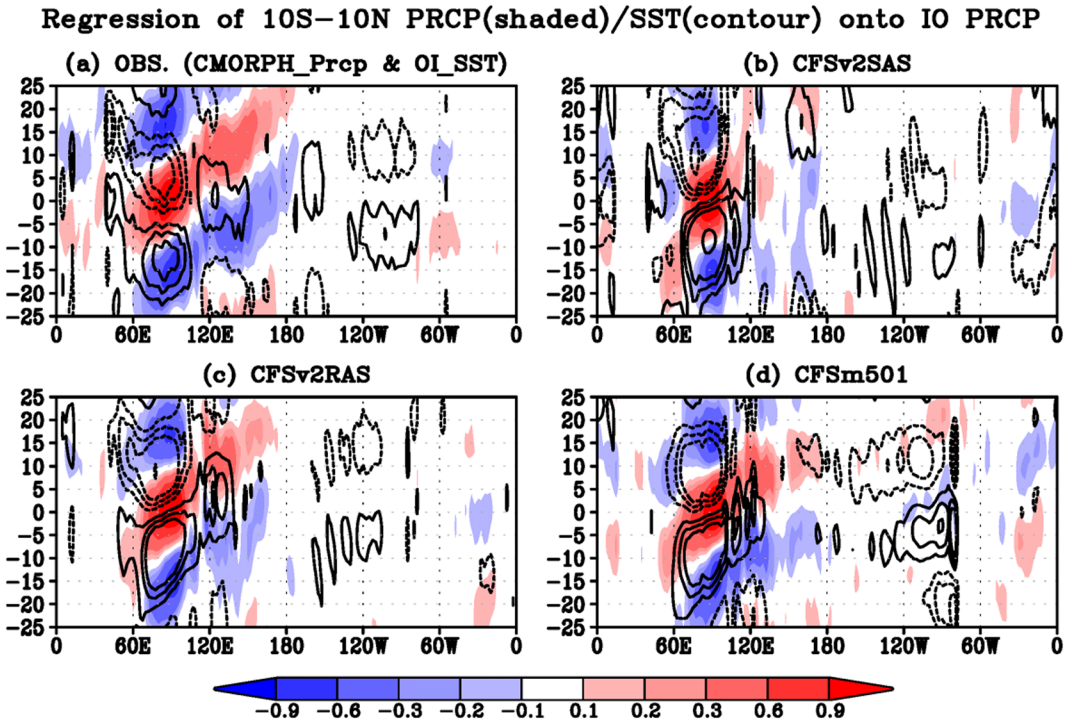

Figure 1. November–April lag-longitude diagram of 10°S to 10°N averaged intraseasonal (20–100-day filtered) precipitation anomalies (colors) and SST anomalies (contours) regressed against the Indian Ocean precipitation (70–100°E, 10°S to 10°N) for (a) observations (CMORPH precipitation and OI SST), (b) CFSv2SAS, (c) CFSv2RAS, and (d) CFSm501. SST contours are plotted at −0.09, −0.06, −0.03, −0.02, −0.01, 0.01, 0.02, 0.03, 0.06, and 0.09°C/(mm/day).

propagation bias in CFSv2SAS might be related to its misrepresentation of overlying SSTs. Specifically, in observations, warm SST anomalies corresponding to convective activity in the Indian Ocean were present to the east of the Maritime Continent (e.g., Krishnamurti et al., 1988; Kumar et al., 2013; Shinoda et al., 1998; Figure 1a). This SST signal, however, was absent in CFSv2SAS (Figure 1b). Zhu et al. (2017) further found that the misrepresented SST conditions ahead of convections in CFSv2SAS could be attributed to its simulation bias in surface latent heat fluxes that were affected by surface winds in both zonal and meridional directions.

When the atmospheric convection scheme in CFSv2SAS is replaced with the RAS scheme (i.e., CFSv2RAS), the zonal propagation of MJO convections was significantly better reproduced (Figure 1c). For CFSv2RAS, the phase relationships among precipitations, low-level winds, SSTs, and surface heat fluxes associated with the MJO were all realistic, as demonstrated in Zhu et al. (2017). In CFSm501, the MJO (particularly the zonal propagation of its associated convection) was also well simulated, which is significantly better than CFSv2SAS (Figure 1d vs. Figure 1b) and has a similar fidelity as CFSv2RAS despite some difference in fine structures (Figure 1d vs. Figure 1c). The comparison among the three CFSv2 configurations confirms a previous finding, that is, among various model configuration factors, the atmospheric convection parametrization is the foremost for simulations of the MJO (Zhang et al., 2006).

While the above validation suggests that CFSv2RAS and CFSm501 can realistically capture the observed propagation of MJO convections, they are not guaranteed to achieve a realistic simulation of associated oceanic variability, for example, the simulation of intraseasonal SSS variability. Figure 2 presents the spatial distribution of intraseasonal SSS variations in simulations by CFSv2RAS and CFSm501 and the observational counterpart based on Aquarius, with climatological SSS distributions superimposed. Note that the intraseasonal SSS variations are related not only to the MJO but also to other factors like ocean internal variability in the form of eddies and instability waves. In Aquarius observations (Figure 2a), larger intraseasonal SSS variations are present over the central-eastern tropical Indian Ocean (including the Bay of Bengal) and the western equatorial Pacific Ocean where the amplitude of variation can reach 0.2 psu (and even larger in parts of

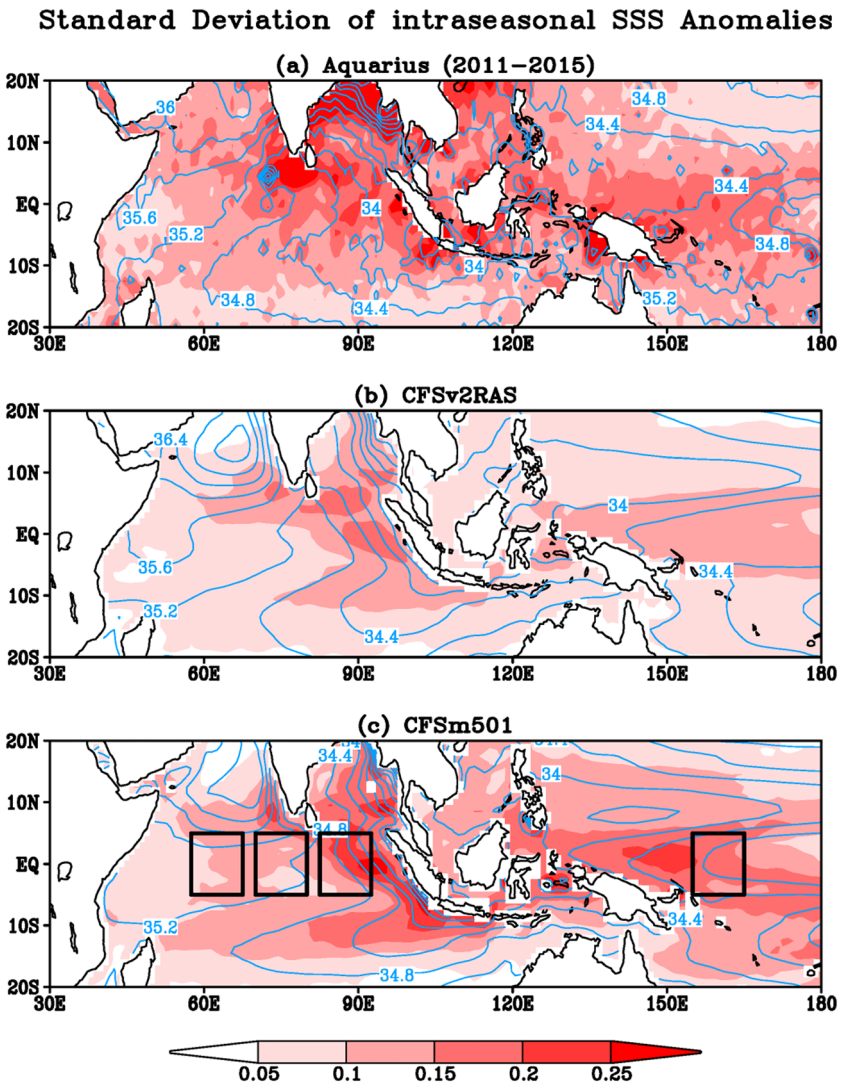

Figure 2. Standard deviation of intraseasonal (20–100-day filtered) SSS anomalies (psu) in (a) Aquarius, (b) CFSv2RAS, and (c) CFSm501. The superimposed contours are climatological SSS (contour interval: 0.4 psu). The four black boxes in Figure 2c are used for analysis in Figure 4.

the Indian basin). The observed spatial pattern is generally captured by CFSv2RAS (Figure 2b vs. Figure 2a), but the amplitude is clearly too weak over the whole tropical Indian and western Pacific region. In particular, over the central-eastern tropical Indian and western equatorial Pacific Oceans, the SSS variation magnitude is 0.1–0.15 psu in CFSv2RAS (Figure 2b), which is around 40–50% weaker than the Aquarius counterpart. In CFSm501 (Figure 2c) that has 1-m vertical resolution near the ocean surface, the spatial pattern of intraseasonal SSS variations is similar to that in Aquarius (Figure 2a) and CFSv2RAS (Figure 2b), but its simulated magnitude demonstrates significant improvements over CFSv2RAS (Figure 2c vs. Figure 2b). Over the central-eastern tropical Indian and western equatorial Pacific Oceans, for example, the magnitude of intraseasonal SSS variations in CFSm501 is around 0.2 psu, which is comparable to the Aquarius estimate. Thus, the commonly used 10-m vertical resolution is not fine enough for a realistic simulation of intraseasonal SSS variability, and the 1-m vertical resolution generally has the capability. Our experiments with only two choices of vertical resolutions (i.e., 10- and 1-m), however, are too limited to provide a more definite requirement for an oceanic vertical resolution to realistically capture the intraseasonal SSS variability. In addition, both simulations clearly underestimate the intraseasonal SSS variability over the northern Bay of Bengal and the northern South China Sea, which

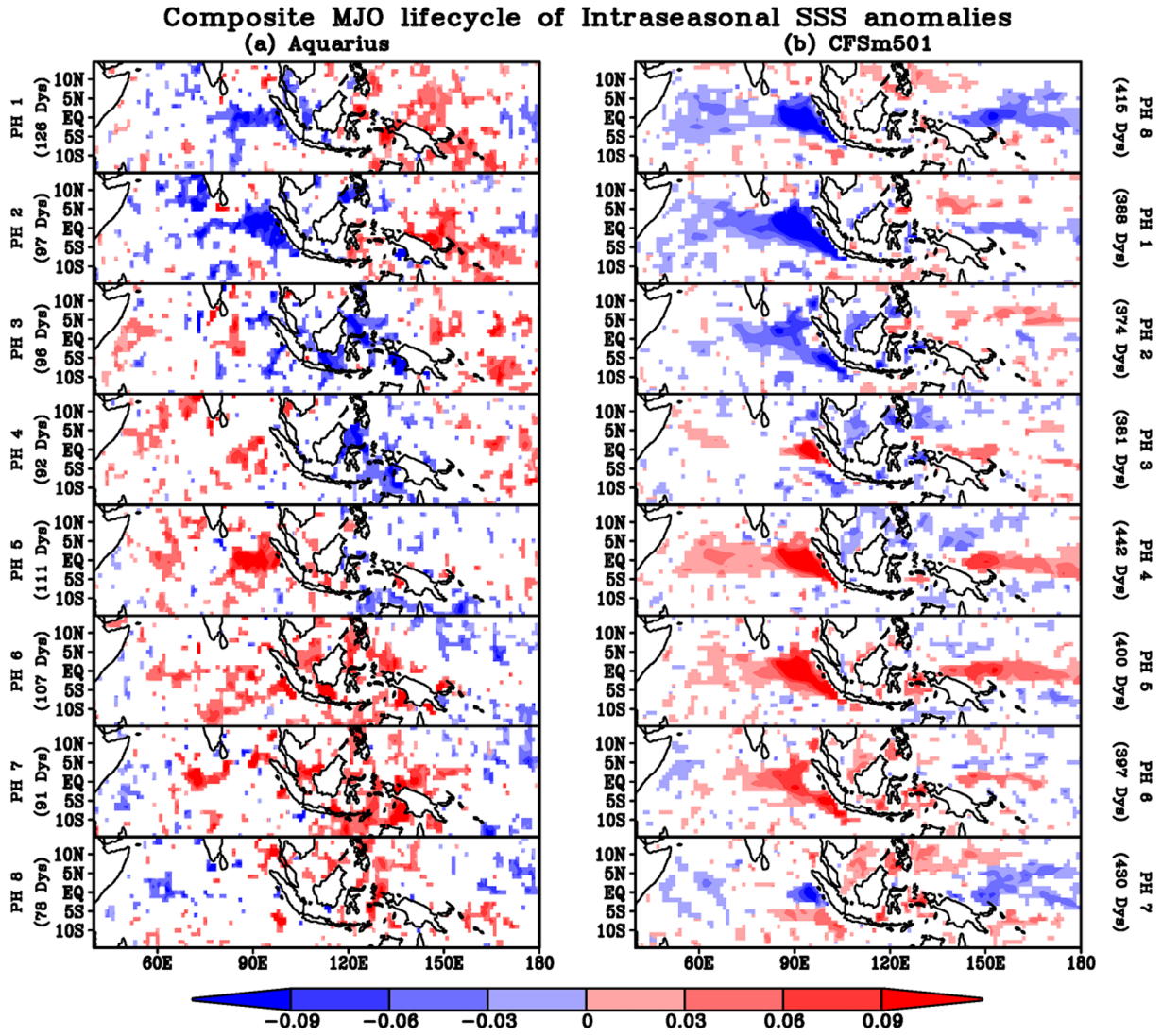

Figure 3. Composite MJO lifecycle of intraseasonal SSS anomalies (psu) in (a) Aquarius observations and (b) CFSm501. For each phase, the composite value is the average of the days when the MJO is in a particular phase and the MJO amplitude is greater than 1, which range from 78 days for Phase 8 (374 days for Phase 2) to 126 days for Phase 1 (442 days for Phase 4) in Aquarius (CFSm501). Values in shadings are significant at the 90% level based on two-tailed Student *t* test.

might be related to factors like unrealistic local salinity front (see contours in Figure 2 over the northern Bay of Bengal), river discharge plume, or mesoscale eddies.

Figure 3 further illustrates the intraseasonal SSS evolution over the composite MJO cycle in CFSm501 and compares it with its Aquarius (Lagerloef, 2012; Yueh, 2013) counterpart. Similar calculations were also performed by Guan et al. (2014) (their Figure 2) for the Aquarius SSS based on a shorter period (i.e., August 2011 to May 2013) and by Zhu and Kumar (2019) (their Figure 3) for the CFSv2RAS simulation. As pointed out previously by Zhu and Kumar (2019), the Aquarius-based analyses of Guan et al. might include large uncertainties because of a relatively short SSS record (around 22 months) applied for their MJO composites. For example, while the near 4-year Aquarius SSS record presents a clear eastward-propagating feature over the composite MJO cycle (Figure 3a), the propagating signal is not well organized in Guan et al. (2014) (their Figure 2), which, instead, is dominated by stationary oscillations. CFSm05 (Figure 3b) realistically captures the SSS eastward-propagating feature over the composite MJO cycle. In comparison with CFSv2RAS (Figure 3b in Zhu and Kumar, 2019), the magnitude of composite SSS anomalies in CFSm501 (Figure 3b) is stronger and closer to the Aquarius estimate (Figure 3a), which is consistent with the variance comparison made in

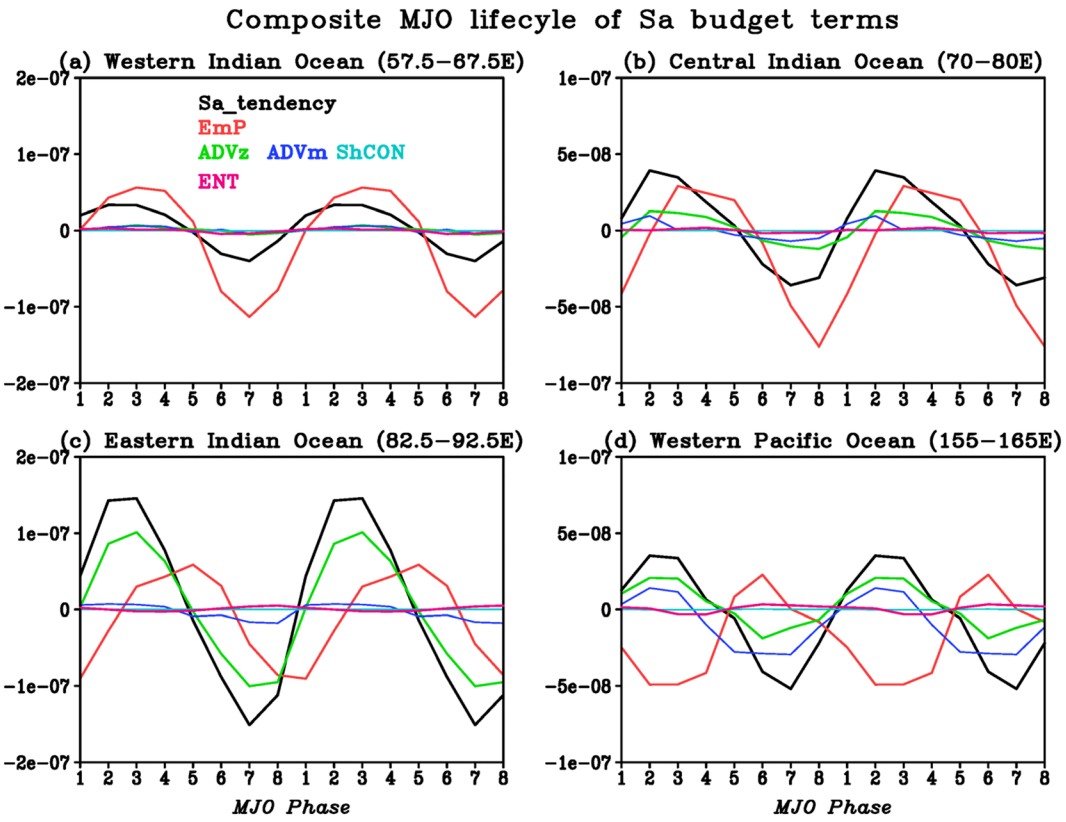

Figure 4. Composite MJO lifecycle of upper ocean salinity budget terms in CFSm501 for (a) the western Indian Ocean (57.5–67.5°E, 5°S to 5°N), (b) the central Indian Ocean (70–80°E, 5°S to 5°N), (c) the eastern Indian Ocean (82.5–92.5°E, 5°S to 5°N), and (d) the western Pacific Ocean (155–165°E, 5°S to 5°N). Sa_tendency (black), EmP (red), ADVz (green), ADVm (blue), ENT (magenta), and ShCON (aqua) respectively stand for budget terms related to tendency, E − P, zonal advection, meridional advection, vertical entrainment, and stratified shear flow convergence.

Figure 2. Therefore, with the adoption of the RAS convection scheme and the 1-m vertical resolution near the ocean surface, CFSm501 demonstrates high fidelity in simulating the MJO-related SSS variability. In the following analysis, we will further investigate the mechanisms attributed to the MJO-associated SSS variability in CFSm501.

When compared against the intraseasonal convection (Figure S2) over the composite MJO cycle, the above intraseasonal SSS signal (Figure 3) roughly follows the propagation of convections in both observation and CFSm501. This relationship, in a qualitative sense, seems to suggest an important role played by the freshwater flux in modulating the MJO-related SSS variability (e.g., Grunseich et al., 2013). Over some regions (e.g., the eastern Indian and western Pacific Oceans), however, the relationship between precipitation and SSS seems more complex, suggesting a possible contribution from ocean dynamics in the SSS variability (e.g., Guan et al., 2014; Matthews et al., 2010).

To provide a more quantitative description of the influence of factors (e.g., surface freshwater fluxes and ocean dynamics) contributing to the intraseasonal salinity variability in CFSm501, a budget analysis (Equation 1; Cronin & McPhaden, 1998) is performed for the mixed layer salinity. The mechanisms for the MJO-related SSS variability in CFSm501 are investigated by Figure 4, which illustrates composite MJO lifecycle of upper-ocean salinity budget terms averaged over four regions in the equatorial Indian and Pacific Oceans (the same regions defined in Guan et al., 2014). The analyses extend the observational counterpart of Guan et al. (2014; Figure 3) by including the explicit contributions from ocean dynamics. Another difference from Guan et al. is that the tendency of salinity other than salinity itself is presented in this analysis. Note that in their illustrations, leads/lags must be considered to identify a causal linkage when examining phase relations between salinity and other budget terms; the calculations presented here, however, could directly give a quantitative description of contributions by different factors.

First, we make a more careful comparison with the observational analyses by Guan et al. (2014). In the western Indian Ocean (Figure 4a), the MJO-related SSS anomalies are dominantly controlled by the E − P forcing despite a small mismatch in their peaks, and contributions from ocean dynamics are generally negligible. The nearly in-phase relation between SSS tendency and E − P is consistent with the near-quadrature relation between SSS and E − P in Guan et al. (2014). In the central Indian Ocean (Figure 4b), the mismatch between the peaks of E − P flux and salinity tendency becomes larger, but the E − P forcing is still a major contribution to the SSS anomalies. The peak mismatch seems to correspond to a complex phase relationship between observational E − P and salinity anomalies suggested by Guan et al. (2014), who concluded a different phase lag during the MJO wet versus dry phases. Besides, in this region, the role of zonal advection term becomes evident, but contributions from other oceanic terms, including meridional advection, vertical entrainment, and stratified shear flow convergence, are still small.

In the eastern Indian Ocean (Figure 4c), the contribution from the zonal advection term becomes even larger and replaces the E − P flux as the dominant term. The E − P flux term becomes in a quadrature relation with the salinity tendency, which is consistent with the nearly in-phase relation between E − P and salinity in Guan et al. (2014). The contribution from the meridional advection term also becomes nonnegligible, while those from other terms are still small. In the western Pacific Ocean (Figure 4d), ocean dynamics also play a dominant role in the local SSS changes, with the contribution by zonal advection complemented by the meridional advection term. For the E − P flux, as in Guan et al. (2014), it plays a complex role: It is generally in an opposite phase with the salinity tendency during Phases 1–6, but in the same phase during Phases 7–8.

Overall, it is encouraging that in CFSm501 the roles of E − P in the MJO-related SSS anomalies over the Indo-Pacific basin are consistent with the observational findings by Guan et al. (2014). Particularly, the comparison between the four regions suggests that different factors play different roles. Moving eastwards from the western Indian Ocean (Figure 4a) to the western Pacific Ocean (Figure 4d), for example, the E − P flux becomes less important in contributing the local MJO-related SSS changes, which even makes a negative contribution in the western Pacific Ocean during the MJO wet phase. Our further diagnostics also suggest that over all the four regions, the dominant contribution to E − P is from the precipitation (P) component (Figure S4). On the other hand, when moving eastwards, the role of ocean dynamics becomes more important, which is consistent with the inference by Matthews et al. (2010) and Guan et al. (2014). Specifically, while the zonal advection term is negligible in the western Indian Ocean (Figure 4a), it plays a dominant role in the eastern Indian (Figure 4c) and western Pacific Oceans (Figure 4d).

4. Conclusion and Discussion

This study is to complement previous observational studies (Grunseich et al., 2013; Guan et al., 2014; Matthews et al., 2010) about the mechanisms of intraseasonal SSS variability over the Indo-Pacific basin. In the previous studies, mostly due to the sparsity of ocean observations (particularly ocean currents), a simplified salinity budget equation, ignoring the contribution from ocean dynamics, was used, and mechanisms were suggested qualitatively based on the relationship between salinity and E − P anomalies associated with the MJO. Despite the efforts, inconsistencies were reported by the studies about roles of E − P versus ocean dynamics in the MJO-related SSS variability over the region.

In this study, by explicitly calculating the contributions from ocean dynamics, a more quantitative description of salinity/freshwater budgets related to the MJO was made based on outputs from a modified CFSv2. Compared to the operational CFSv2 (Saha et al., 2014), the CFSv2 applied in this study has a different atmospheric convection scheme and a higher vertical resolution in the near-surface ocean. The modifications resulted in more realistic simulations of the MJO and intraseasonal SSS variability. The budget analysis about the MJO-related SSS variability indicates a strong regional dependency on physical processes controlling the local SSS variability. Particularly, as moving eastwards from the western Indian Ocean to the western Pacific Ocean, the E − P flux becomes less important in controlling the local MJO-related SSS changes, and ocean dynamics, in contrast, become more important. A similar finding was also achieved in forced ocean-alone experiments (e.g., Li et al., 2015). Besides, by comparing with previous observational studies (e.g., Guan et al., 2014), it is also encouraging to see that CFSm501 generally captured the relation between the MJO-related E − P and SSS anomalies over the Indo-Pacific basin.

Our diagnostics also suggest that the modified CFSv2 might be a good tool to address other salinity-related scientific questions. A particular example will be how salinity (BL) could feedback onto the MJO evolution, a hypothesis being investigated by the Dynamics of the Madden-Julian Oscillation (DYNAMO; Yoneyama et al., 2013) field campaign. So far, some studies (e.g., Drushka et al., 2014; Guan et al., 2014) have implied that salinity can feedback onto MJO variability by modulating upper ocean stratification variability (e.g., BL) and further intraseasonal SST. However, it seems challenging to discover direct evidence proving such feedback because of significant model biases (Zhu & Kumar, 2019). The modified CFSv2 with improved salinity and BL (not shown) simulations could be a better candidate for such explorations, which are hard to be addressed by forced ocean-alone experiments. Besides, we also plan to utilize the model for some observing system simulation experiment (OSSE) studies in support of TPOS 2020 (Cravatte et al., 2016).

Acknowledgments
The authors are grateful to Drs. Bin Guan, Tony Lee, Dongxiao Zhang, Meghan Cronin, Aneesh Subramanian, Kelvin Richards, Charlotte DeMott, and Bohua Huang for their comments. Funding for this study is provided by NOAA's Climate Program Office through the Climate Variability and Predictability (CVP) and Modeling, Analysis, Predictions, and Projections (MAPP) programs and a NASA Ocean Salinity Science Team grant (NNX17AK09G). The rainfall data are available through Joyce et al., (2004), the wind data are available through Saha et al. (2010), the SSS data are available through Yueh (2013), and the daily RMM index values (including the phase and magnitude of the MJO) are obtained from the Center for Australian Weather and Climate Research (http://www.bom.gov.au/climate/mjo/).

References

Annamalai, H., Murtugudde, R., Potemra, J., Xie, S., Liu, P., & Wang, B. (2003). Coupled dynamics over the Indian Ocean: Spring initiation of the zonal mode. *Deep Sea Research, Part II*, *50*(12), 2305–2330.

Bellenger, Y. N., Takayabu, T. U., & Yoneyama, K. (2010). Role of diurnal warm layers in the diurnal cycle of convection over the tropical Indian Ocean during MISMO. *Monthly Weather Review*, *138*(6), 2426–2433. https://doi.org/10.1175/2010MWR3249.1

Bernie, D. J., Woolnough, S. J., & Slingo, J. M. (2005). Modeling diurnal and intraseasonal variability of the ocean mixed layer. *Journal of Climate*, *18*(8), 1190–1202. https://doi.org/10.1175/JCLI3319.1

Cravatte, S., Kessler, W. S., Smith, N., Wijffels, S. E., & Contributing Authors (2016). First Report of TPOS 2020. GOOS-215, TPOS 2020, 200 pp. Available online at TPOS2020.org/first-report/.

Cronin, M. F., & McPhaden, M. J. (1998). Upper ocean salinity balance in the western equatorial Pacific. *Journal of Geophysical Research*, *103*(C12), 27,567–27,587. https://doi.org/10.1029/98JC02605

DeMott, C. A., Klingaman, N. P., & Woolnough, S. J. (2015). Atmosphere-ocean coupled processes in the Madden-Julian oscillation. *Reviews of Geophysics*, *53*, 1099–1154. https://doi.org/10.1002/2014RG000478

Drushka, K., Sprintall, J., Gille, S., & Wijffels, S. (2012). In situ observations of Madden-Julian oscillation mixed layer dynamics in the Indian and western Pacific Oceans. *Journal of Climate*, *25*(7), 2306–2328. https://doi.org/10.1175/JCLI-D-11-00203.1

Drushka, K., Sprintall, J., & Gille, S. T. (2014). Subseasonal variations in salinity and barrier-layer thickness in the eastern equatorial Indian Ocean. *Journal of Geophysical Research: Oceans*, *119*, 805–823. https://doi.org/10.1002/2013JC009422

Flatau, M., Flatau, P. J., Phoebus, P., & Niler, P. P. (1997). The feedback between equatorial convection and local radiative and evaporative processes: The implications for intraseasonal oscillations. *Journal of the Atmospheric Sciences*, *54*(19), 2373–2386. https://doi.org/10.1175/1520-0469(1997)054<2373:TFBECA>2.0.CO;2

Font, J., Boutin, J., Reul, N., Spurgeon, P., Ballabrera-Poy, J., Chuprin, A., et al. (2013). SMOS first data analysis for sea surface salinity determination. *International Journal of Remote Sensing*, *34*(9–10), 3654–3670. https://doi.org/10.1080/01431161.2012.716541

Fu, X., Yang, B., Bao, Q., & Wang, B. (2008). Sea surface temperature feedback extends the predictability of tropical intraseasonal oscillation. *Monthly Weather Review*, *136*(2), 577–597. https://doi.org/10.1175/2007MWR2172.1

Ge, X., Wang, W., Kumar, A., & Zhang, Y. (2017). Simulations of SST diurnal and intraseasonal variability in an oceanic general circulation model. *Journal of Climate*, *30*(11), 3963–3978. https://doi.org/10.1175/JCLI-D-16-0689.1

Grunseich, G., Subrahmanyam, B., & Wang, B. (2013). The Madden-Julian oscillation detected in Aquarius salinity observations. *Geophysical Research Letters*, *40*, 5461–5466. https://doi.org/10.1002/2013GL058173

Guan, B., Lee, T., Halkides, D. J., & Waliser, D. E. (2014). Aquarius surface salinity and the Madden-Julian oscillation: The role of salinity in surface layer density and potential energy. *Geophysical Research Letters*, *41*, 2858–2869. https://doi.org/10.1002/2014GL059704

Hung, M.-P., Lin, J.-L., Wang, W., Kim, D., Shinoda, T., & Weaver, S. J. (2013). MJO and convectively coupled equatorial waves simulated by CMIP5 climate models. *Journal of Climate*, *26*(17), 6185–6214. https://doi.org/10.1175/JCLI-D-12-00541.1

Inness, P. M., Slingo, J. M., Guilyardi, E., & Cole, J. (2003). Simulation of the Madden-Julian oscillation in a coupled general circulation model. Part II: The role of the basic state. *Journal of Climate*, *17*, 365–382.

Jiang, X., Waliser, D. E., Xavier, P. K., Petch, J., Klingaman, N. P., Woolnough, S. J., et al. (2015). Vertical structure and physical processes of the Madden-Julian oscillation: Exploring key model physics in climate simulations. *Journal of Geophysical Research: Atmospheres*, *120*, 4690–4717. https://doi.org/10.1002/2014JD022374

Joyce, R. J., Janowiak, J. E., Arkin, P. A., & Xie, P. (2004). CMORPH: A method that produces global precipitation estimates from passive microwave and infrared data at high spatial and temporal resolution. *Journal of Hydrometeorology*, *5*(3), 487–503. https://doi.org/10.1175/1525-7541(2004)005<0487:CAMTPG>2.0.CO;2

Krishnamurti, T. N., Oosterhof, D. K., & Metha, A. V. (1988). Air-sea interaction on the timescale of 30–50 days. *Journal of the Atmospheric Sciences*, *45*(8), 1304–1322. https://doi.org/10.1175/1520-0469(1988)045<1304:AIOTTS>2.0.CO;2

Kumar, A., Zhang, L., & Wang, W. (2013). Sea surface temperature-precipitation relationship in different reanalyses. *Monthly Weather Review*, *141*(3), 1118–1123. https://doi.org/10.1175/MWR-D-12-00214.1

Lagerloef, G. (2012). Aquarius/SAC-D: The First Science Data. 7th Aquarius/SAC-D Science Meeting. 11–13 April 2012, Buenos Aires, Argentina.

Li, Y., & Han, W. (2016). Causes for intraseasonal sea surface salinity variability in the western tropical Pacific Ocean and its seasonality. *Journal of Geophysical Research: Oceans*, *121*, 85–103. https://doi.org/10.1002/2015JC011413

Li, Y., Han, W., & Lee, T. (2015). Intraseasonal sea surface salinity variability in the equatorial Indo-Pacific Ocean induced by Madden-Julian oscillations. *Journal of Geophysical Research: Oceans*, *120*, 2233–2258. https://doi.org/10.1002/2014JC010647

Li, Y., Han, W., Shinoda, T., Wang, C., Lien, R. C., Moum, J. N., & Wang, J. W. (2013). Effects of the diurnal cycle in solar radiation on the tropical Indian Ocean mixed layer variability during wintertime Madden-Julian oscillations. *Journal of Geophysical Research: Oceans*, *118*, 4945–4964. https://doi.org/10.1002/jgrc.20395

Lukas, R., & Lindstrom, E. (1991). The mixed layer of the western equatorial Pacific Ocean. *Journal of Geophysical Research*, *96*(S01), 3343–3357. https://doi.org/10.1029/90JC01951

Madden, R. A., & Julian, P. R. (1971). Detection of a 40–50 day oscillation in the zonal wind in the tropical Pacific. *Journal of the Atmospheric Sciences*, *28*(5), 702–708. https://doi.org/10.1175/1520-0469(1971)028<0702:DOADOI>2.0.CO;2

Maes, C., Picaut, J., & Belamari, S. (2005). Importance of the salinity barrier layer for the buildup of El Nino. *Journal of Climate*, *18*(1), 104–118.

Matthews, A. J., Singhruck, P., & Heywood, K. J. (2010). Ocean temperature and salinity components of the Madden-Julian oscillation observed by Argo floats. *Climate Dynamics*, *35*(7-8), 1149–1168. https://doi.org/10.1007/s00382-009-0631-7

Moorthi, S., & Suarez, M. J. (1992). Relaxed Arakawa-Schubert: A parameterization of moist convection for general circulation models. *Monthly Weather Review*, *120*(6), 978–1002. https://doi.org/10.1175/1520-0493(1992)120<0978:RASAPO>2.0.CO;2

Pan, H.-L., & Wu, W.-S. (1995). Implementing a mass flux convection parameterization package for the NMC medium-range forecast model. NMC Office Note 409, 39 pp.

Pegion, K., & Kirtman, B. (2008). The impact of air-sea interactions on the predictability of the tropical intraseasonal oscillation. *Journal of Climate*, *21*(22), 5870–5886. https://doi.org/10.1175/2008JCLI2209.1

Roemmich, D., & Owens, W. B. (2000). The Argo Project: Global ocean observations for understanding and prediction of climate variability. *Oceanography*, *13*(2), 45–50. https://doi.org/10.5670/oceanog.2000.33

Saha, S., Moorthi, S., Wu, X., Wang, J., Nadiga, S., Tripp, P., et al. (2014). The NCEP Climate Forecast System version 2. *Journal of Climate*, *27*(6), 2185–2208. https://doi.org/10.1175/JCLI-D-12-00823.1

Saha, S., Moorthi, S., Pan, H.-L., Wu, X., Wang, J., Nadiga, S., et al. (2010). The NCEP climate forecast system reanalysis. *Bulletin of the American Meteorological Society*, *91*(8), 1015–1058. https://doi.org/10.1175/2010BAMS3001.1

Schmitt, R. W. (2008). Salinity and the global water cycle. *Oceanography*, *21*(1), 12–19. https://doi.org/10.5670/oceanog.2008.63

Seo, H., Xie, S. P., Murtugudde, R., Jochum, M., & Miller, A. J. (2009). Seasonal effects of Indian Ocean freshwater forcing in a regional coupled model. *Journal of Climate*, *22*(24), 6577–6596. https://doi.org/10.1175/2009JCLI2990.1

Shinoda, T., & Hendon, H. H. (1998). Mixed layer modeling of intraseasonal variability in the tropical western Pacific and Indian Oceans. *Journal of Climate*, *11*, 2668–2685.

Shinoda, T., & Hendon, H. H. (2001). Upper-ocean heat budget in response to the Madden-Julian oscillation in the western equatorial Pacific. *Journal of Climate*, *14*(21), 4147–4165. https://doi.org/10.1175/1520-0442(2001)014<4147:UOHBIR>2.0.CO;2

Shinoda, T., Hendon, H. H., & Glick, J. (1998). Intraseasonal variability of surface fluxes and sea surface temperature in the tropical western Pacific and Indian Oceans. *Journal of Climate*, *11*(7), 1685–1702. https://doi.org/10.1175/1520-0442(1998)011<1685:IVOSFA>2.0.CO;2

Shinoda, T., Jensen, T., Flatau, M., Han, W., & Wang, C. (2013). Large-scale oceanic variability associated with the Madden-Julian oscillation during the CINDY/DYNAMO field campaign from satellite observations. *Remote Sensing*, *5*(5), 2072–2092. https://doi.org/10.3390/rs5052072

Sprintall, J., & Tomczak, M. (1992). Evidence of the barrier layer in the surface layer of the tropics. *Journal of Geophysical Research*, *97*(C5), 7305–7316. https://doi.org/10.1029/92JC00407

Vitart, F., Woolnough, S., Balmaseda, M. A., & Tompkins, A. M. (2007). Monthly forecast of the Madden-Julian oscillation using a coupled GCM. *Monthly Weather Review*, *135*(7), 2700–2715. https://doi.org/10.1175/MWR3415.1

Waliser, D. E., Lau, K. M., & Kim, J.-H. (1999). The influence of coupled SSTs on the Madden-Julian oscillation: A model perturbation experiment. *Journal of the Atmospheric Sciences*, *56*(3), 333–358. https://doi.org/10.1175/1520-0469(1999)056<0333:TIOCSS>2.0.CO;2

Wang, B., & Rui, H. (1990). Synoptic climatology of transient tropical intraseasonal convection anomalies: 1975–1985. *Meteorology and Atmospheric Physics*, *44*(1–4), 43–61. https://doi.org/10.1007/BF01026810

Wang, W., Hung, M.-P., Weaver, S. J., Kumar, A., & Fu, X. (2014). MJO prediction in the NCEP Climate Forecast System version 2. *Climate Dynamics*, *42*, 2509–2520.

Wheeler, M. C., & Hendon, H. H. (2004). An all-season real-time multivariate MJO index: Development of an index for monitoring and prediction. *Monthly Weather Review*, *132*(8), 1917–1932. https://doi.org/10.1175/1520-0493(2004)132<1917:AARMMI>2.0.CO;2

Woolnough, S. J., Vitart, F., & Balmaseda, M. A. (2007). The role of the ocean in the Madden-Julian oscillation: Implications for MJO prediction. *Quarterly Journal of the Royal Meteorological Society*, *133*(622), 117–128. https://doi.org/10.1002/qj.4

Yoneyama, K., Zhang, C., & Long, C. N. (2013). Tracking pulses of the Madden-Julian oscillation. *Bulletin of the American Meteorological Society*, *94*, 1871–1891.

Yueh, S. (2013). Aquarius CAP Algorithm and Data User Guide, version 2.0, Jet Propulsion Laboratory, California Institute of Technology, Pasadena, Calif.

Zhang, C., Dong, M., Gualdi, S., Hendon, H. H., Maloney, E. D., Marshall, A., et al. (2006). Simulations of the Madden-Julian oscillation in four pairs of coupled and uncoupled global models. *Climate Dynamics*, *27*(6), 573–592. https://doi.org/10.1007/s00382-006-0148-2

Zhang, X., Lu, Y., Thompson, K. R., Jiang, J., & Ritchie, H. (2010). Tropical Pacific Ocean and the Madden-Julian oscillation: Role of wind and buoyancy forcing. *Journal of Geophysical Research*, *115*, C05022. https://doi.org/10.1029/2009JC005734

Zhang, Y., Hung, M.-P., Wang, W., & Kumar, A. (2019). Role of SST feedback in the prediction of the boreal summer monsoon intraseasonal oscillation. *Climate Dynamics*, *53*(7–8), 3861–3875. https://doi.org/10.1007/s00382-019-04753-w

Zhu, J., Huang, B., Zhang, R. H., Hu, Z. Z., Kumar, A., Balmaseda, M. A., et al. (2014). Salinity anomaly as a trigger for ENSO events. *Scientific Reports*, *4*(1), 6821. https://doi.org/10.1038/srep06821

Zhu, J., & Kumar, A. (2019). Role of sea surface salinity feedback in MJO predictability: A study with CFSv2. *Journal of Climate*, *32*(18), 5745–5759. https://doi.org/10.1175/JCLI-D-18-0755.1

Zhu, J., Wang, W., & Kumar, A. (2017). Simulations of MJO propagation across the maritime continent: Impacts of SST feedback. *Journal of Climate*, *30*(5), 1689–1704. https://doi.org/10.1175/JCLI-D-16-0367.1